化 学 学 报
ACTA CHIMICA SINICA

研究论文
Article

DOI: 10.6023/A16100542

# 具有三维导电网络结构的锡纳米颗粒/石墨烯纳米片复合电极材料的储镁性能研究

张长欢[a] 李念武[a] 姚胡蓉[a,b] 刘琳[a,b] 殷雅侠*[,a,b] 郭玉国*[,a,b]

([a]中国科学院化学研究所 中国科学院分子纳米结构与纳米技术重点实验室 北京 100190)

([b]中国科学院大学 化学与化工学院 北京 100049)

**摘要** 镁二次电池具有安全性高、价格低廉等优点, 是一种具有潜在应用前景的高能量密度电池体系. 目前, 镁二次电池的研究重点之一是寻找合适的电极材料. 最近, 我们通过水热和热处理相结合的方法成功制备了具有三维导电网络结构的锡纳米颗粒/石墨烯纳米片复合电极材料. 研究发现, 在石墨烯的三维导电网络片层上, 均匀分布了粒径小于 100 nm 的锡纳米颗粒. 将锡纳米颗粒/石墨烯纳米片复合材料作为镁二次电池电极材料, 当电流密度为 15 mA•g$^{-1}$ 和 300 mA•g$^{-1}$ 时, 首次放电容量分别达到了 545.4 mAh•g$^{-1}$ 和 238.8 mAh•g$^{-1}$, 经过 150 圈后, 容量保持率达到了 93%, 库伦效率为 99%, 表现出了较高的电化学活性. 研究还发现, 镁离子嵌入复合材料中形成镁锡合金, 当镁离子脱出后, 再次形成锡纳米颗粒/石墨烯纳米片复合电极材料, 镁离子的脱出和嵌入具有很高的可逆性. 这对未来研究设计高性能镁离子电极材料具有十分重要的意义.

**关键词** 储镁材料; 镁二次电池; 纳米复合材料; 三维导电网络; 锡纳米颗粒; 石墨烯纳米片

# Synthesis of Sn Nanoparticles/Graphene Nanosheet Hybrid Electrode Material with Three-Dimensional Conducting Network for Magnesium Storage

Zhang, Changhuan[a] Li, Nianwu[a] Yao, Hurong[a,b] Liu, Lin[a,b]
Yin, Yaxia*[,a,b] Guo, Yuguo*[,a,b]

([a] *CAS Key Laboratory of Molecular Nanostructure and Nanotechnology*, *Institute of Chemistry*, *Chinese Academy of Sciences* (*CAS*), *Beijing 100190*, *China*)

([b] *School of Chemistry and Chemical Engineering*, *University of Chinese Academy of Sciences*, *Beijing 100049*, *China*)

**Abstract** Rechargeable magnesium (Mg) batteries have attracted research attention as one promising alternative for energy storage because of abundant raw materials. However, the strong electrostatic interaction between bivalent Mg-ions and host lattices often cause sluggish solid state diffusion of Mg-ion within the local crystal structure and consequently prevent reversible insertion/extraction of Mg-ion. Thus much more effort has been paid to develop suitable electrode materials with Mg-ion storage capability. This paper reports the synthesis of Sn nanoparticles/reduced-graphene-oxide nanosheet hybrid nanocomposite (Sn/rGO), by simple hydrothermal method and subsequent thermal treatment. Transmission electron microscopy (TEM) clearly shows that in the as-synthesized Sn/rGO powder Sn nanoparticles are well crystallized, and X-ray diffraction (XRD) pattern was consistent well with tetragonal Sn. Thermogravimetric analysis (TG) suggested that the mass percentage of Sn is *ca*. 82.3 wt% in the Sn/rGO nanocomposite, very close to the design ratio of *ca*. 83.4 wt%. As Mg-ion battery anode, the Sn/rGO electrode material exhibit a high initial discharge specific capacity (545.4 mAh•g$^{-1}$ at 15 mA•g$^{-1}$), good reversible ability and rate performance. The impressive electrochemical property could be attributed to the unique structure of Sn/rGO, in which the three-dimensional (3D) conducting network of rGO can effectively prevent the aggregation of Sn nanoparticles and alleviate the serious volume variation of Sn during repeated discharging/charging process, as well as facilitate the fast access of electrons and Mg-ion to improve kinetics for Mg-ion insertion/extraction. *Ex situ* XRD and SEM characterization were performed to investigate the electrochemical evolution of Sn/rGO electrode at different discharging/charging states. It is found that upon magnesiation crystalline $Mg_2Sn$ appears and subsequently disappears during de-magnesiation process, which indicates the good electrochemical activity of Sn nanoparticles in Sn/rGO hybrid nanocomposite for magnesium storage. Our result will open new avenue to develop high-efficient magnesium storage material for rechargeable Mg batteries.

* E-mail: yxyin@iccas.ac.cn, ygguo@iccas.ac.cn; Tel.: 010-82617069; Fax: 010-82617069
Received October 13, 2016; published December 19, 2016.

**Supporting information** for this article is available free of charge via the Internet at http://sioc-journal.cn.

Project supported by the National Natural Science Foundation of China (Grant Nos. 51225204, 21303222, and 21127901) and the "Strategic Priority Research Program" of the Chinese Academy of Sciences (Grant No. XDA09010100).

项目受国家自然科学基金(Nos. 51225204, 21303222, 21127901)和中国科学院战略性先导科技专项(XDA09010100)资助.

  

**Keywords** magnesium storage; rechargeable magnesium battery; nanocomposite; conducting network; tin; graphene

## 1 Introduction

Rechargeable batteries have become one of the key systems for energy storage. In particular, lithium-ion batteries have been widely applied for most portable electronic devices as power sources.[1~3] However, rechargeable batteries with much high safety, low cost, and high volumetric energy density are recently being required for large scale applications.[4,5] Magnesium (Mg) is more stable in ambient atmosphere and abundant in the earth crust compared with lithium (Li). In addition, the specific volumetric capacity of Mg can reach 3833 mAh•cm$^{-3}$, which is higher than that of Li (2046 mAh•cm$^{-3}$).[6,7] So the rechargeable Mg batteries are considered as one potential solution for the ever-increasing demand for large-scaled energy storage.[8~10] And the increasing attention has been paid to rechargeable Mg batteries after the pioneering work of Aurbach's group.[11 ~ 13] However, the development of Mg-ion batteries has been limited from serious challenge in selecting suitable electrode materials because the strong electrostatic interaction between bivalent Mg-ions and host lattices often causes slow solid state diffusion of Mg-ion within the local crystal structure, thus prevents reversible insertion/extraction of Mg-ion. Some progress has been achieved toward designing electrode materials.[11,14 ~ 26] Among potential electrode materials for magnesium storage, Sn is of great interest as the Mg-ion anode with a relatively high theoretical capacity (903 mAh•g$^{-1}$), originating from the alloying reaction with Mg, Sn is electrochemically stable in the electrolyte.[17,27] However, alloy anode materials usually suffer from serious volume change and electrochemical aggregation during Mg insertion and extraction, resulting in the electrode pulverization, rapid capacity fading, and a strong charge-rate dependence on reversible capacity.[17]

Graphene has been widely used as the highly efficient three-dimensional conducting network due to its high electronic conductivity to improve the performance of electrode materials suffering from the limited kinetics of lithium storage. Additionally, large surface area of graphene nanosheet can guarantee a good distribution of active nanoparticles on its surface and its flexibility can effectively buffer the volume varation of active nanoparticles during cycles.[28] In this work, we synthesized the Sn nanoparticles/reduced-graphene-oxide nanosheet hybrid nanocomposite (Sn/rGO) as the anode material for Mg-ion batteries by a simple two-step method, composed of hydrothermal (1st step) and thermal treatment (2nd step). After the hydrothermal process, the obtained GO and $SnO_2$ were reduced into rGO and Sn nanoparticles by thermal reduction, respectively. As the anode materials of Mg-ion battery, the Sn/rGO nanocomposite delivers a high initial discharge specific capacity (545.4 mAh•g$^{-1}$ at 15 mA•g$^{-1}$ and 238.8 mAh•g$^{-1}$ at 300 mA•g$^{-1}$), good reversible ability, and rate performance. The excellent electrochemical property of Sn/rGO nanocomposite comes from its unique structure, in which the folded rGO facilitates the penetration of electrolyte into the hybrid structure to enhance Mg-ion accessibility. In addition, the rGO skeleton could maintain the integrity and improve the conductivity of the electrode system, holding the small particles in electrical contact with the current collector.

## 2 Results and discussion

The synthesized Sn/rGO nanocomposite exhibits typical morphology of Sn nanoparticles grown on the folded rGO sheets (Figure 1), and most of Sn nanoparticles are almost one hundred nanometer. SEM image shows a relatively uniform distribution of Sn particles throughout the sample. There was no impurity phase in the synthesized Sn/rGO, as revealed from the XRD pattern (Figure 2a). Well-crystallized Sn is identified with a tetragonal crystal structure (JCPDS Card No. 04-0673). In addition, the typical High-resolution (HR) TEM image (Figure 2b), TEM image (Figure 2c), and corresponding elemental mapping images (Figure 2d~2e) also show that crystallized Sn nanoparticles with the size of about one hundred nanometer are uniformly dispersed on graphene conducting network. Without introducing GO during the synthesizing process, we obtained the mixture of crystallized $SnO_2$ (JCPDS Card No. 88-0287) and Sn (JCPDS Card No. 04-0673) as confirmed from XRD result (Figure S1). And the prepared mixture shows microparticle morphology (Figure S2). These results suggest that GO could play important role on the reduction of $SnO_2$ into Sn and preventing the progressive growth of particles during synthesis process.

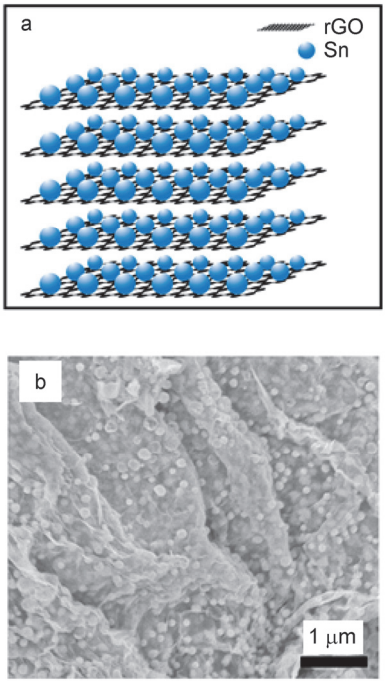


**Figure 1** (a) Schematic illustration and (b) SEM image of the Sn/rGO nanocomposite

Thermogravimetric analysis (TG) was performed to obtain the Sn content in the Sn/rGO nanocomposite (Figure

  

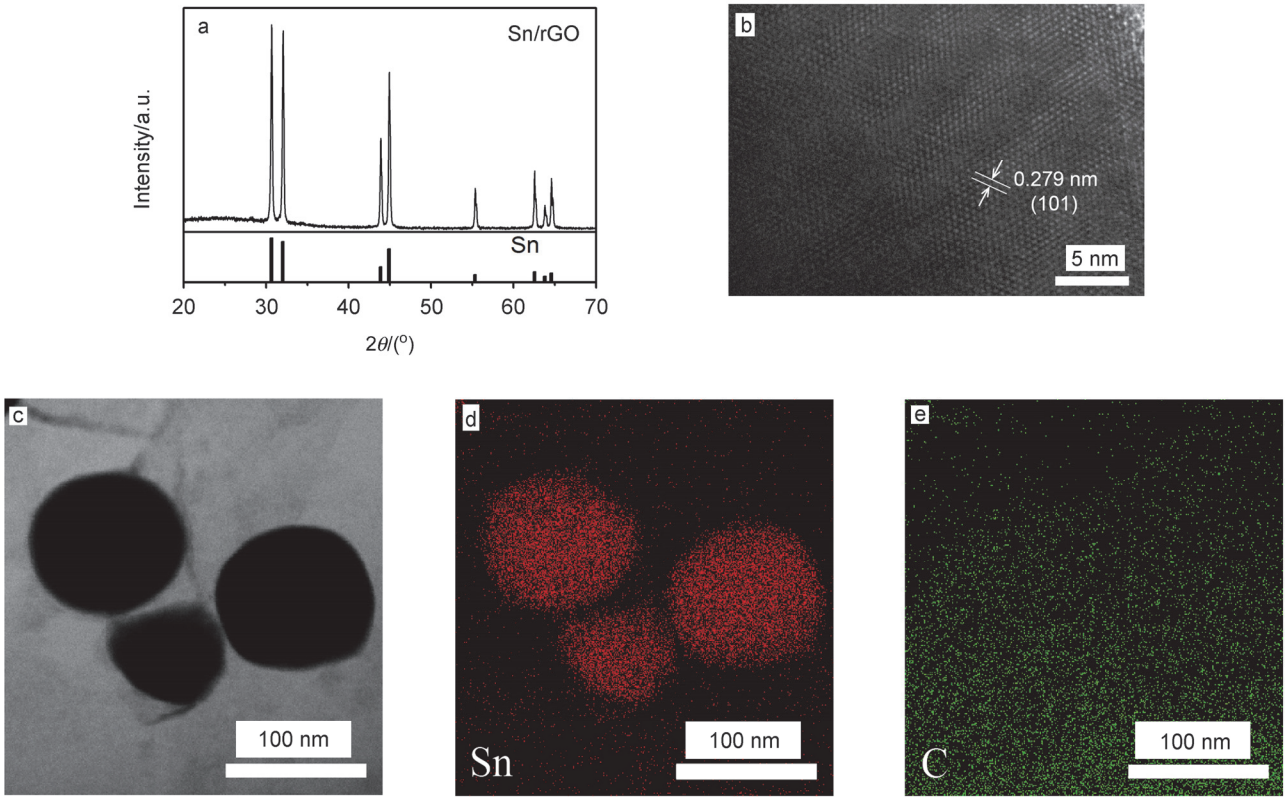


**Figure 2** (a) XRD pattern and (b) HRTEM image of Sn/rGO nanocomposite. (c) TEM image of Sn/rGO nanocomposite and corresponding elemental mapping images of (d) tin and (e) carbon

3). There are one-step weight loss and two-step weight gain observed in the TG curve. The sharp weight gain occurred in the temperature ranges of 200～450 ℃. This may be mainly due to the oxidation reaction of Sn to $SnO_2$. The major weight loss from 450 ℃ to 600 ℃ may come from the oxidation reaction of rGO. When heating to 600 ℃, the further weight gain was observed, suggested that Sn nanoparticles were continuously oxided into $SnO_2$ from 200 to 750 ℃. After 750 ℃, the weight of sample was constant. This gave a yield of about 104.5 wt% because the Sn/rGO nanocomposite eventually evolved into $SnO_2$ in the air after the whole thermal treatment. Based on TG results, the mass percentage of Sn is caculated to be *ca*. 82.3 wt% in Sn/rGO nanocomposite, very close to the design ratio of *ca*. 83.4 wt%.

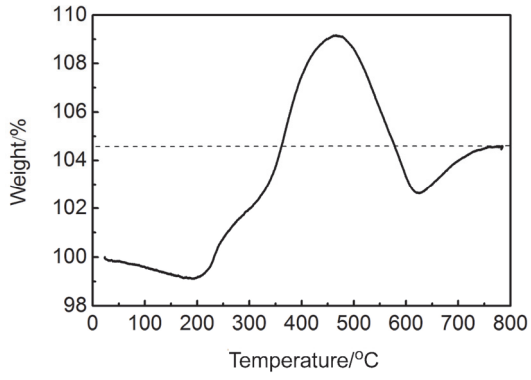


**Figure 3** TG curve of Sn/rGO nanocomposite

In order to investigate the electrochemical performance of the Sn/rGO nanocomposite, we assembled the testing cells with a Sn/rGO electrode as the working electrode and Mg metal as the counter electrode separated by a membrane. Figure 4a exhibits the cyclic voltammograms (CVs) of the Sn/rGO electrode in a half-cell for the first 10 cycles within the potential range of 0～0.8 V vs. $Mg^{2+}$/Mg at a scan rate of 0.01 mV•$s^{-1}$. In the first cycle, there are two anodic peaks centered at 0.31 and 0.41 V respectively. And the peak at 0.41 V is no longer present in subsequent cycles. In the subsequent scanning process, the Sn/rGO electrode exhibited relatively high symmetric cathodic/anodic peak with Mg insertion (0～0.17 V) and deinsertion (0.23～0.44 V), confirming the high electrochemical activity and good reversiblity of Sn/rGO nanocomposite to magnesium storage. The current density of cathodic/anodic peak shows a trend of rise during initial several cycles. It might be associated with an activation process during the initial discharging-charging process. Figure 4b displays the galvanostatic discharge/charge profiles of the Sn/rGO electrode for the first cycle at a current density of 15 mA•$g^{-1}$. The Sn/rGO electrode delivers capacities of 545.4 and 426.0 mAh•$g^{-1}$ for the first discharge and charge process at a current density of 15 mA•$g^{-1}$. We used commercial Sn powder (*ca*. 200 mesh) as the control material for magnesium storage. No obvious voltage plateau and capacity could be observed for large-sized Sn powder, indicating the serious size-dependent magnesium storage of Sn. During the initial ten discharge/charge process, the specific capacities show a trend of first rise and then fall (Figure 4c),

  

consistent with the CV curves. The Sn/rGO electrode delivers a discharge capacity of 238.8 mAh•g$^{-1}$ as the current density subsequently increases to 300 mA•g$^{-1}$ (Figure 4c), which is better than previously reported performance of Sn nanoparticles.[17] Then the discharge capacity first fall and then rise to 221.1 mAh•g$^{-1}$ after 150 cycles. This corresponds to capacity retention of 93%, indicating the good cycling stability. The average Coulombic efficiency is above 99% during cycles. The rate capability of the Sn/rGO electrode under various current densities is further shown in Figure 4d. The Sn/rGO electrode exhibits the discharge capacities of 550.4, 369.6, 326.6, 271.4, 203.5, and 298.1 mAh•g$^{-1}$ at the current densities of 15, 30, 60, 150, 300 and 30 mA•g$^{-1}$, respectively. The results show the relatively good reversible ability.[14~16]

An *ex situ* X-ray diffraction (XRD) study was performed to investigate the electrochemical evolution of Sn/rGO electrode at different discharging/charging states (Figure 5). XRD patterns of the pristine Sn/rGO electrode are indexed to the tetragonal phase Sn without any impurity peaks. Upon magnesiation, crystalline peaks associated with the formation of $Mg_2Sn$ (JCPDS card No. 06-0190), corresponding to the alloying reaction of Sn with Mg, were observed along with remnant Sn peaks. No metallic Mg was observed in the spectra. And for the de-magnesiation sample, crystalline $Mg_2Sn$ disappear and simultaneously crystalline Sn phase re-form. After the second discharging process (Mg insertion again), diffraction peaks corresponding to $Mg_2Sn$ were clearly observed again, albeit some weak peaks of crystallized Sn still exist. This results indicate the highly reversibility of Sn nanoparticles for magnesium storage. In addition, there exist trace impurity phase in the magnesiation and de-magnesiation sample. These impurity phases may come from the side reaction of Cu current collector with 0.4 mol/L PhMgCl-$AlCl_3$ electrolyte, which is illustrated from CVs curves and *ex situ* XRD spectra of (Supplementary Figure S3 and Figure S4) Sn/rGO nanocomposite with stainless steel foil as current collector. No obvious impurity was observed for Sn/rGO electrode with stainless steel foil upon discharging/charging process, suggesting the minimal side reaction between stainless steel and PhMgCl-$AlCl_3$ electrolyte.

Figure 6 shows SEM images of the pristine Sn/rGO electrode, magnesiated Sn/rGO electrode, and de-magnesiated Sn/rGO electrode. No distinct morphology change of the Sn/rGO nanocomposite are observed during cycles. It indicated that the rGO can effectively prevent the electrochemical aggregation of Sn nanoparticles, and buffer the volume change of alloy reaction during the charging and discharging process, as well as maintains the structural integrity and conductivity of the electrode system. These unique attributes of rGO could enhance the electrochemical properties of Sn towards magnesium storage.

## 3 Conclusions

As described in this paper, a hybrid nanocomposite of Sn nanoparticles/reduced-graphene-oxide nanosheet with 3D conducting network was designed as the anode material for rechargeable Mg batteries. Such hybrid nanostructure

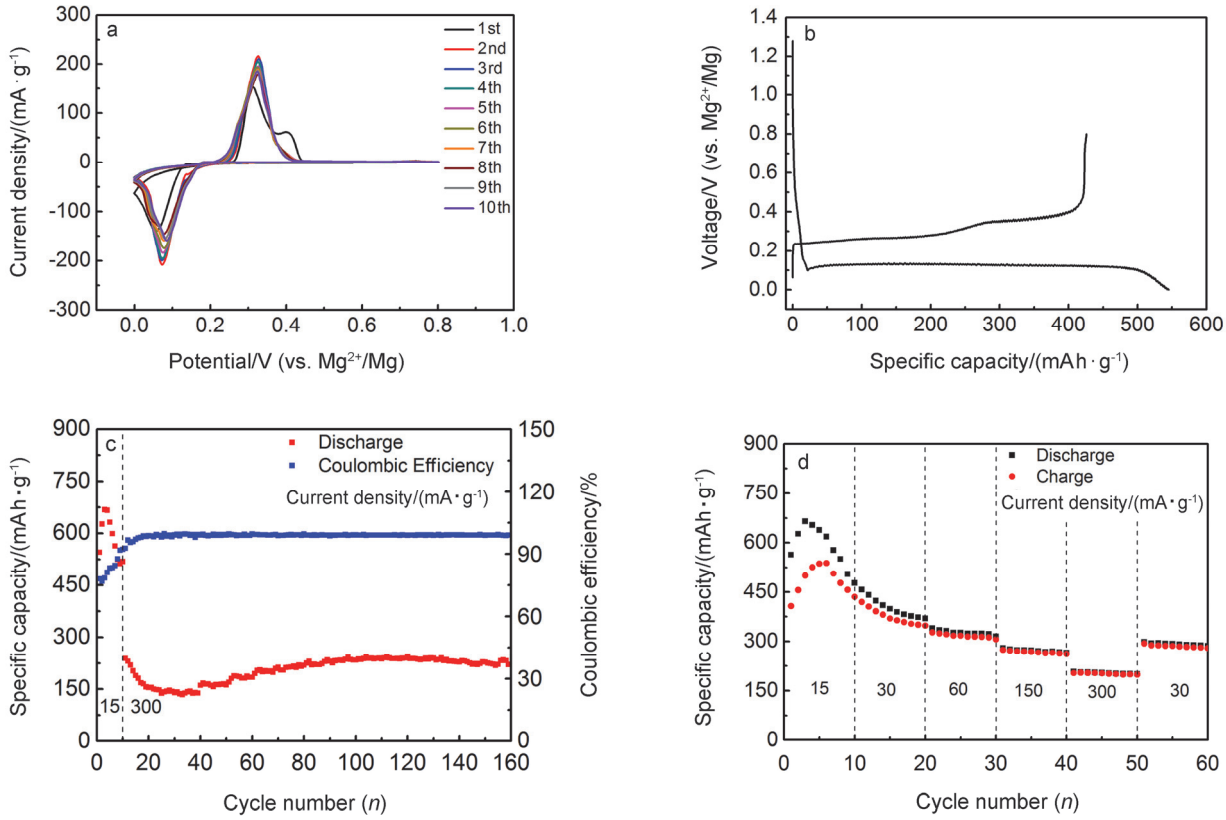


**Figure 4** (a) CV curves of the Sn/rGO electrode for the first 10 cycles at a scan rate of 0.01 mV•s$^{-1}$ in a potential range of 0~0.8 V vs. $Mg^{2+}$/Mg. (b) Galvanostatic charge/discharge profiles of the Sn/rGO electrode for the first cycle at a current density of 15 mA•g$^{-1}$. (c) Cycling performance and (d) rate capability of the Sn/rGO electrode

  

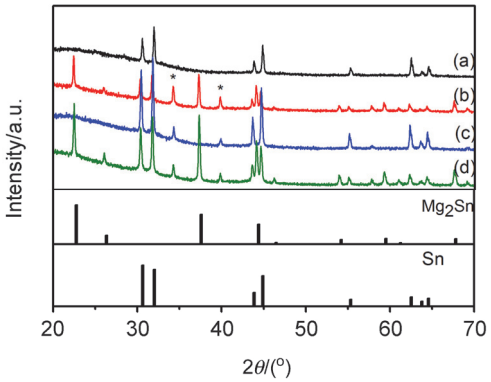


**Figure 5** XRD spectra of the (a) pristine Sn/rGO electrode, (b) first discharged electrode, (c) first recharged electrode, and (d) second discharged electrode. * are the impurity phases

can effectively facilitate the penetration of electrolyte and thus enhance Mg-ion accessibility. The introduction of rGO can effectively buffer the volume variation and prevent the aggregation of Sn nanoparticles during the Mg insertion and extraction. Therefore, the rGO framework could maintain the structural integrity and improve the conductivity of the electrode system. The resultant Sn/rGO nanocomposite delivers a high first discharge specific capacity of 238.8 mAh•g$^{-1}$ at the current density of 300 mA•g$^{-1}$. In addition, the Sn/rGO nanocomposite exhibits good capacity retention after 150 cycles even at high current density of 300 mA•g$^{-1}$, with a high Coulombic efficiency of 99%. These results will open new options to development of Mg-ion anode material for rechargeable Mg batteries.

## 4 Experimental

### 4.1 Preparation of Sn/rGO nanocomposite

All of the reagents were of analytical grade purity and used without any further treatment. Graphite oxide (GO) was synthesized according to the modified Hummer's method starting from natural graphite flake (natural, −325, Alfa Aesar).[29] The GO was obtained after ultrasonic and centrifuge processes, which was washed with deionized water and further dispersed into deionized water. The concentration of GO dispersion was estimated to be about 4.3 mg•mL$^{-1}$.

Tin chloride dehydrate ($SnCl_2$•$2H_2O$, AR, Sinopharm Chemical Reagent Co., Ltd) was firstly added to *N*,*N*-dimethylformamide (DMF, AR, Beijing Chemical Works) to obtain the concentration of 26.6 mmol•L$^{-1}$ with magnetic stirring for 1 h, and then appropriate volume of GO dispersion was added to the solution. The weight ratio of $SnCl_2$•$2H_2O$ and GO was 10∶1. The mixed solution was firstly heated at 80 ℃ for 4 h and then transferred to a Teflon lined stainless steel autoclave for hydrothermal reaction at 120 ℃ for 12 h. The obtained products were washed with ethanol for at least three times and then drying at 80 ℃ for 12 h. The dried powders were transferred into a tube furnace and were heated at 500 ℃ for 5 h under the protection of reductive gas (5% $H_2$ and 95% Ar) to yield Sn/rGO nanocomposite.

### 4.2 Preparation of electrolyte

The electrolyte in this study was prepared in two steps according to previous reports[30]. First, 0.26668 g Aluminium trichloride ($AlCl_3$, anhydrous, 99.99%, Sigma-Aldrich) was very slowly added to 3 mL of Tetrahydrofuran (THF, anhydrous, ⩾99.9%, Sigma-Aldrich) under vigorous stirring to form $AlCl_3$-THF solution. In the second step, 2 mL of Phenyl magnesium chloride (PhMgCl, 2 mol/L solution in THF, Sigma-Aldrich) solution was added drop by drop in 3 mL of $AlCl_3$-THF solution. The final solution was stirred at least 24 h prior to use. It should be addressed that the previous two steps are exothermic reactions. A stirring stage with a cooling system is strongly

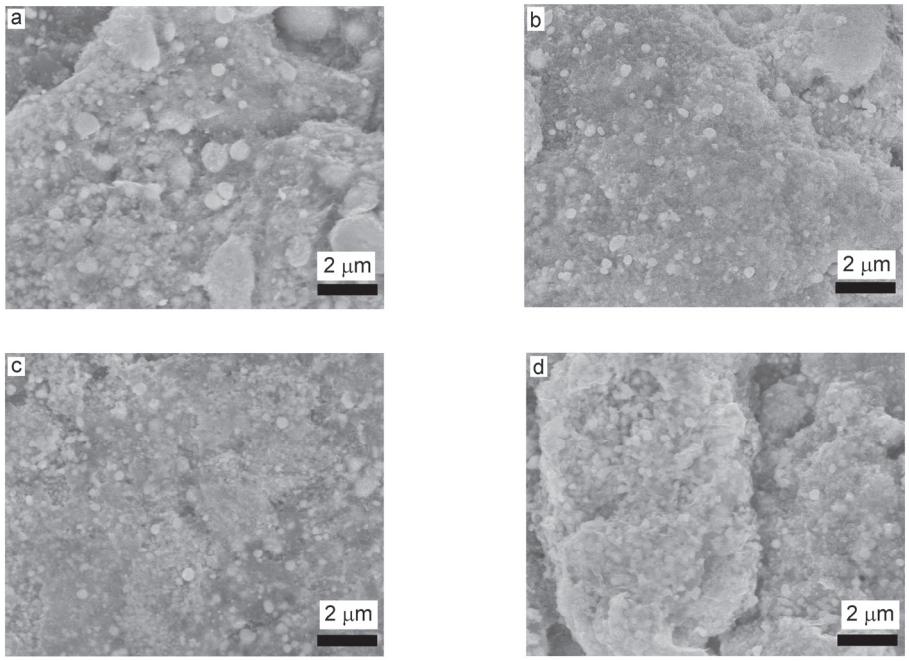


**Figure 6** SEM images of (a) pristine Sn/rGO electrode, (b) first discharged electrode, (c) first recharged electrode, and (d) second discharged electrode

  

suggested for the mixing process. Since the electrolyte is sensitive to moisture, all the processes should be performed under argon in a glove box (＜0.1 ppm of water and oxygen).

### 4.3 Cells assembling and electrochemical measurements

The electrodes were composed of Sn/rGO nanocomposite, super P (SP), and poly(vinyl difluoride) (PVDF) binder with a weight ratio of 80∶10∶10, which were coated onto a piece of copper foil (99.6%, Goodfellow) and was punched into disk electrodes after drying at 80 ℃ overnight. The loading mass of the active materials is approximately 2.0 mg•cm$^{-2}$. CR2032 coin cells were assembled with Whatman borosilicate glass fiber paper as the separator, magnesium foil as the counter electrode, and 180 μL of 0.4 mol/L PhMgCl-$AlCl_3$ in THF as the electrolyte in an argon-filled glove box.

The cycling performance and the rate capability were measured by an Arbin BT2000 system in the potential range of 0 to 0.8 V versus $Mg^{2+}$/Mg. The current density was calculated on the basis of the weight of the Sn/rGO nanocomposite in the electrode. Cyclic voltammograms (CVs) test was carried out using an Autolab electrochemical workstation (PG302N) in the same potential range with a scan rate of 0.01 mV•s$^{-1}$ (vs. $Mg^{2+}$/Mg). All electrochemical measurements were carried out at 25 ℃.

### 4.4 Preparation of *ex-situ* XRD and SEM samples

For preparing the magnesiated sample, the pristine Sn/rGO electrode was discharged to 0 V vs. Mg at a constant current of 15 mA•g$^{-1}$. For de-magnesiated sample, the pristine Sn/rGO electrode was charged to 0.8 V vs. Mg. All the cells were disassembled inside an argon-filled glove box and the magnesiated or de-magnesiated electrodes were washed repeatedly with THF and dried at 25 ℃ overnight to remove excess electrolyte bound to the surface and obtained XRD and SEM samples. Before XRD test, the nanocomposite was scraped off from the current collector of the washed magnesiated and de-magnesiated electrode using a clean razor blade.

## References


[1] Ye, Y.; Zhu, J.; Yao, Y.; Wang, Y.; Wu, P.; Tang, Y.; Zhou, Y.; Lu, T. *Acta Chim. Sinica* **2015**, *73*, 151. (叶亚, 朱婧怡, 姚依男, 王雨果, 吴平, 唐亚文, 周益明, 陆天虹, 化学学报, **2015**, *73*, 151.)

[2] Lyu, Z.; Feng, R.; Zhao, J.; Fan, H.; Xu, D.; Wu, Q.; Yang, L.; Chen, Q.; Wang, X.; Hu, Z. *Acta Chim. Sinica* **2015**, *73*, 1013. (吕之阳, 冯瑞, 赵进, 范豪, 徐丹, 吴强, 杨立军, 陈强, 王喜章, 胡征, 化学学报, **2015**, *73*, 1013.)

[3] Qiu, Z. P.; Zhang, Y. J.; Xia, S. B.; Dong, P. *Acta Chim. Sinica* **2015**, *73*, 992. (邱振平, 张英杰, 夏书标, 董鹏, 化学学报, **2015**, *73*, 992.)

[4] Luo, F.; Zheng, J. Y.; Chu, G.; Liu, B. N.; Zhang, S. L.; Li, H.; Chen, L. Q. *Acta Chim. Sinica* **2015**, *73*, 808. (罗飞, 郑杰允, 褚赓, 刘柏男, 张素林, 李泓, 陈立泉, 化学学报, **2015**, *73*, 808.)

[5] Yan, Y.; Yin, Y. X.; Guo, Y. G.; Wan, L. J. *Sci. China-Chem.* **2014**, *57*, 1564.

[6] Matsui, M. *J. Power Sources* **2011**, *196*, 7048.

[7] Ling, C.; Banerjee, D.; Matsui, M. *Electrochim. Acta* **2012**, *76*, 270.

[8] Saha, P.; Datta, M. K.; Velikokhatnyi, O. I.; Manivannan, A.; Alman, D.; Kumta, P. N. *Prog. Mater. Sci.* **2014**, *66*, 1.

[9] Yoo, H. D.; Shterenberg, I.; Gofer, Y.; Gershinsky, G.; Pour, N.; Aurbach, D. *Energ. Environ. Sci.* **2013**, *6*, 2265.

[10] Shterenberg, I.; Salama, M.; Gofer, Y.; Levi, E.; Aurbach, D. *Mrs. Bull.* **2014**, *39*, 453.

[11] Aurbach, D.; Lu, Z.; Schechter, A.; Gofer, Y.; Gizbar, H.; Turgeman, R.; Cohen, Y.; Moshkovich, M.; Levi, E. *Nature* **2000**, *407*, 724.

[12] Aurbach, D.; Weissman, I.; Gofer, Y.; Levi, E. *Chem. Rec.* **2003**, *3*, 61.

[13] Chusid, O.; Gofer, Y.; Gizbar, H.; Vestfrid, Y.; Levi, E.; Aurbach, D.; Riech, I. *Adv. Mater.* **2003**, *15*, 627.

[14] Levi, E.; Gofer, Y.; Aurbach, D. *Chem. Mater.* **2010**, *22*, 860.

[15] Imamura, D.; Miyayama, M.; Hibino, M.; Kudo, T. *J. Electrochem. Soc.* **2003**, *150*, A753.

[16] Tao, Z. L.; Xu, L. N.; Gou, X. L.; Chen, J.; Yuan, H. T. *Chem. Commun.* **2004**, *18*, 2080.

[17] Singh, N.; Arthur, T. S.; Ling, C.; Matsui, M.; Mizuno, F. *Chem. Commun.* **2013**, *49*, 149.

[18] Shao, Y.; Gu, M.; Li, X.; Nie, Z.; Zuo, P.; Li, G.; Liu, T.; Xiao, J.; Cheng, Y.; Wang, C.; Zhang, J. G.; Liu, J. *Nano Lett.* **2014**, *14*, 255.

[19] Wu, N.; Lyu, Y. C.; Xiao, R. J.; Yu, X.; Yin, Y. X.; Yang, X. Q.; Li, H.; Gu, L.; Guo, Y. G. *Npg Asia Mater.* **2014**, *6*, e120.

[20] Wu, N.; Yang, Z. Z.; Yao, H. R.; Yin, Y. X.; Gu, L.; Guo, Y. G. *Angew. Chem. Int. Ed.* **2015**, *54*, 5757.

[21] He, D.; Wu, D.; Gao, J.; Wu, X.; Zeng, X.; Ding, W. *J. Power Sources* **2015**, *294*, 643.

[22] Kim, C.; Phillips, P. J.; Key, B.; Yi, T.; Nordlund, D.; Yu, Y.-S.; Bayliss, R. D.; Han, S.-D.; He, M.; Zhang, Z.; Burrell, A. K.; Klie, R. F.; Cabana, J. *Adv. Mater.* **2015**, *27*, 3377.

[23] Liang, Y.; Yoo, H. D.; Li, Y.; Shuai, J.; Calderon, H. A.; Hernandez, F. C. R.; Grabow, L. C.; Yao, Y. *Nano Lett.* **2015**, *15*, 2194.

[24] Murgia, F.; Stievano, L.; Monconduit, L.; Berthelot, R. *J. Mater. Chem. A* **2015**, *3*, 16478.

[25] Su, S.; Huang, Z.; Nuli, Y.; Tuerxun, F.; Yang, J.; Wang, J. *Chem. Commun.* **2015**, *51*, 2641.

[26] Huang, J.; Poyraz, A. S.; Takeuchi, K. J.; Takeuchi, E. S.; Marschilok, A. C. *Chem. Commun.* **2016**, *52*, 4088.

[27] Malyi, O. I.; Tan, T. L.; Manzhos, S. *J. Power Sources* **2013**, *233*, 341.

[28] Xin, S.; Guo, Y. G.; Wan, L. J. *Acc. Chem. Res.* **2012**, *45*, 1759.

[29] Hummers, W. S.; Offeman, R. E. *J. Am. Chem. Soc.* **1958**, *80*, 1339.

[30] Mizrahi, O.; Amir, N.; Pollak, E.; Chusid, O.; Marks, V.; Gottlieb, H.; Larush, L.; Zinigrad, E.; Aurbach, D. *J. Electrochem. Soc.* **2008**, *155*, A103.


(Cheng, B.; Fan, Y.)

  